Inorg. Chem. **2007**, *46*, 5727–5733

New $[LNi^{II}_2]^+$ Complexes Incorporating 2-Formyl or 2,6-Diformyl-4-methyl Phenol as Inhibitors of the Hydrolysis of the Ligand L^{3-}: Ni···Ni Ferromagnetic Coupling and $S = 2$ Ground States

Alok Ranjan Paital,[‡] Wing Tak Wong,[†] Guillem Aromí,*[,§] and Debashis Ray*[,‡]

Department of Chemistry, Indian Institute of Technology, Kharagpur 721 302, India, Department of Chemistry, The University of Hong Kong, Pokfulam Road, Pokfulam, Hong Kong SAR, P.R. China, and Departament de Química Inorgànica, Universitat de Barcelona, Diagonal 647, 08028 Barcelona, Spain

Received March 14, 2007

Reaction of the dinucleating ligand H_3L (2-(2′-hydroxyphenyl)-1,3-bis[4-(2-hydroxyphenyl)-3-azabut-3-enyl]-1,3-imidazolidine) with $Ni(NO_3)_2 \cdot 6H_2O$ produces the dimer of monomers $[Ni(HL1)]_2(NO_3)_2 \cdot 4H_2O$ (**1**·$4H_2O$) following the hydrolysis of H_3L. If the reaction occurs in the presence of 2-formylphenol (Hfp) or 2,6-diformyl-4-methylphenol (Hdfp), this hydrolysis is prevented by incorporation of these co-ligands into the structure and stabilization of the new complexes $[Ni_2L(fp)(H_2O)] \cdot 3H_2O$ (**2**·$3H_2O$) and $[Ni_2L(dfp)] \cdot 4.5H2O$ (**3**·$4.5H_2O$), respectively. Complexes **2** and **3** may be considered to be structural models of the active site of urease, where coordination of the carbonyl ligand mimics binding of urea. In complex **2**, coordination of terminal water reproduces the binding of this substrate of the enzyme to the active site. In both dinuclear complexes, the Ni^{II} ions are coupled ferromagnetically to yield $S = 2$ ground states, whereas complex **1** exhibits weak intradimer antiferromagnetic exchange through hydrogen bonds. The magnetic data can be modeled by using the Van Vleck equation, incorporating intermolecular interactions, or by diagonalization of a spin Hamiltonian that includes single-ion anisotropy.

Introduction

Of the known nickel metalloenzymes, urease is among of the best studied. It is based on a Ni^{II} dinuclear active site that catalyzes the hydrolysis of urea to carbamate and the ammonium ion.[1,2] From the crystal structure of the enzyme, it is known that the two nickel ions are separated by about 3.5 Å,[3] weakly antiferromagnetically coupled,[4] coordinated to a terminal water molecule and bridged by a hydroxide ion. The substrate (urea) binds to one of the metals through its carbonyl oxygen. Biomimetic studies remain an important tool for understanding the mode of action of the enzyme. They have lead, for instance, to the proposal that the hydrolysis of urea occurs through the nucleophilic attack of a hydroxide ion on the carbonyl carbon atom of the substrate producing ammonia and carbamic acid.[5] We and others have been interested in the dinucleating properties of the ligand H_3L (Scheme 1, 2-(2′-hydroxyphenyl)-1,3-bis[4-(2-hydroxyphenyl)-3-azabut-3-enyl]-1,3-imidazolidine)[6] and its close derivative H_3L' (2-(2′-hydroxyphenyl)-1,3-bis[4-(2-hydroxyphenyl)-4-methyl-3-azabut-3-enyl]-2-methyl-1,3-imidazolidine)[7] for various reasons, including their importance in bioinorganic chemistry, molecular magnetism, or catalysis.[7−12]

* To whom correspondence should be addressed. E-mail: dray@chem.iitkgp.ernet.in.
‡ Indian Institute of Technology
† University of Hong Kong.
§ Universitat de Barcelona.

(1) Halcrow, M. A.; Christou, G. *Chem. Rev.* **1994**, *94*, 2421−2481.
(2) Karplus, P. A.; Pearson, M. A.; Hausinger, R. P. *Acc. Chem. Res.* **1997**, *30*, 330−337.
(3) Jabri, E.; Carr, M. B.; Hausinger, R. P.; Karplus, P. A. *Science* **1995**, *268*, 998−1004.
(4) Clark, P. A.; Wilcox, D. E. *Inorg. Chem.* **1989**, *28*, 1326−1333.
(5) Barrios, A. M.; Lippard, S. J. *J. Am. Chem. Soc.* **2000**, *122*, 9172−9177.
(6) Wong, E.; Liu, S.; Lugger, T.; Hahn, F. E.; Orvig, C. *Inorg. Chem.* **1995**, *34*, 93−101.
(7) Bera, M.; Wong, W. T.; Aromí, G.; Ray, D. *Eur. J. Inorg. Chem.* **2005**, 2526−2535.
(8) Nanda, P. K.; Aromí, G.; Ray, D. *Chem. Commun.* **2006**, 3181−3183.
(9) Nanda, P. K.; Aromí, G.; Ray, D. *Inorg. Chem.* **2006**, *45*, 3143−3145.
(10) Fondo, M.; García-Deibe, A. M.; Corbella, M.; Ruiz, E.; Tercero, J.; Sanmartín, J.; Bermejo, M. R. *Inorg. Chem.* **2005**, *44*, 5011.
(11) Fondo, M.; Ocampo, N.; García-Deibe, A. M.; Corbella, M.; Bermejo, M. R.; Sanmartín, J. *Dalton Trans.* **2005**, 3785.
(12) Fondo, M.; García-Deibe, A. M.; Sanmartín, J.; Bermejo, M. R.; Lezama, L.; Rojo, T. *Eur. J. Inorg. Chem.* **2003**, 3703−3706.

10.1021/ic700496c CCC: $37.00
Published on Web 06/15/2007

Scheme 1

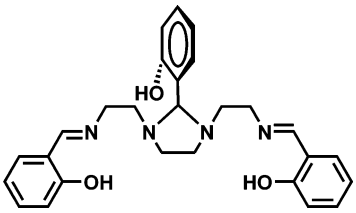

During the course of these investigations, we have observed that in certain conditions, complexation reactions with Mn^{III}, Fe^{III}, Co^{III}, or Cu^{II} leads to the hydrolysis of the imidazolidine ring[13−15] and even the destruction of the imine bond of the heptadentate ligand.[16] The instability of some of the dinuclear Ni^{II} complexes of a related ligand has been reported as well.[17] We have investigated the hydrolysis of H_3L as triggered by Ni^{II} and isolated the complex resulting from the hydrolyzed ligand, H_2L1. The hydrolysis has been prevented by use of the appropriate *o*-formylphenols as co-ligands, namely, 2-formylphenol (Hfp) and 2,6-diformyl-4-methylphenol (Hdfp). Hydroxycarboxaldehydes of this type have been used extensively as precursors in the preparation of more complicated ligands;[18,19] however, their use as exogenous bridging ligands is very uncommon. Reported here are the stable dinuclear Ni^{II} complexes of H_3L resulting from the use of Hfp or Hdfp as co-ligand. These have been isolated and crystallographically characterized, which has allowed a detailed investigation of their magnetic properties.

Results and Discussion

Synthesis and Reactivity. In a previous report, it was noticed by Fondo et al. that a complex with formula $[Ni_2(AcO)L''(H_2O)_2]$ was unstable in solution and produced crystals of the new complex $[Ni_2(o\text{-}OC_6H_3BrCHO)(L'')(H_2O)]$ in low yield (H_3L'' is a ligand like H_3L with Br substituents on the phenols).[17] Since the *o*-formylphenoxide moiety is a product of hydrolysis of $(L'')^{3-}$, this suggests that the decomposition is inhibited by the former through displacement of the AcO^- bridge. Therefore the solution stability of $(L'')^{3-}$ as part of $[Ni^{II}_2]$ complexes depends on the nature of the co-ligands.

We have carried out the reaction of $Ni(NO_3)_2{\cdot}6H_2O$ with H_3L in MeOH and have obtained a 60% yield of the hydrolyzed complex $[Ni(HL1)]_2(NO_3)_2$ (**1**, Scheme 2), which shows that NO_3^- as co-ligand does not prevent the hydrolysis of L^{3-}. However, no sign of the expected coproduct $[Ni_2L(fp)(H_2O)]$ (**2**) was observed, perhaps because of the added stability of **1**, which crystallizes as dimers of mononuclear complexes assembled through H-bonding. The process of hydrolysis, however, was inhibited completely if Hfp was mixed previously with the solution of $Ni(NO_3)_2{\cdot}6H_2O$, presumably leading to the formation of intermediate **A** (Scheme 2), to result in the formation of complex **2** in a 76% yield, after addition of H_3L. Interestingly, the dicarbonyl Hdfp also inhibits the hydrolysis of L^{3-} through a similar process (Scheme 2, path through intermediate **B**) to be found as a tridentate bridging ligand in the new compound $[Ni_2L(dfp)]$ (**3**), obtained in 79%. The formulation of all complexes is consistent with elemental analysis and electrical conductivity data in CH_3CN.

Infrared Spectroscopy. The sharp peak in the IR spectra of complexes **1**, **2**, and **3**, at 1641, 1642, and 1639 cm^{-1} are characteristic of the C═N functionality of the ligands $(L1)^{2-}$ or L^{3-}, respectively. Broad medium bands at 3401, 3267, and 3268 cm^{-1} are observed corresponding to ν(OH) vibrations from lattice water molecules. In addition, complex **1** shows a broad band around 3056 cm^{-1} for the ν(NH) stretching of the amino moieties of the transformed ligand. Complexes **2** and **3** also show sharp bands at 1600 cm^{-1} resulting from the coordinated ν(C═O) functionality of the formyl phenolates.

Description of Structures. Single crystals suitable for X-ray structure determination were obtained by slow evaporation of $MeCN/CH_2Cl_2$ (1:1) solutions of **2** and **3** and of a MeCN solution of **1** in a week. Crystallographic data are summarized in Table 1, and selected interatomic distances and angles are collected in Table 2. ORTEP and other representations of the three compounds are shown on Figures 1−5.

$[Ni(HL1)]_2(NO_3)_2{\cdot}4H_2O$ (1·4H_2O). Complex **1** (Figure 1) is a dimer of Ni^{II} cationic monomers, each with a *cis*-N_4O_2 octahedral coordination sphere provided exclusively by one $(HL1)^{2-}$ hexadentate ligand in the form of five chelate rings. Of these, two are six-membered and three are five-membered. The charge in this complex is compensated by two NO_3^- groups. Both monomers are linked together through two self-complementary H-bonds as established between the phenolic −OH residue of one ligand and the phenoxide O atom of the opposite ligand, having O(1)−O(3) and O(2)−O(4) distances of 2.463(7) and 2.457(7) Å, respectively. In this manner, both monomers are facially disposed so that their four phenolic oxygen atoms display a tetrahedral arrangement. The asymmetric unit contains two $[Ni(HL1)]^+$ units, two NO_3^- anions, and four water molecules of crystallization. The latter are engaged in a 1D network of anion−water hydrogen bonds running along the crystallographic *a*-axis (Figure S1).

$[Ni_2(L)(fp)(H_2O)]{\cdot}3H_2O$ (2·3H_2O). Complex **2** (Figure 2) is a neutral aggregate of two Ni^{II} ions linked together by the action of the N_4O_3 heptadentate ligand L^{3-} (Scheme 1). The bridging function is accomplished by the central imidazolidine group (NCN group) and phenoxide moiety (one μ-O) of L^{3-}, while the imine N atom and the phenoxide O donor at each side of the ligand saturate two additional coordination sites of each Ni^{II} center, respectively. An exogenous bidentate 2-formylphenoxide (fp^-) ligand contributes to the bridging

(13) Bera, M.; Mukhopadhyay, U.; Ray, D. *Inorg. Chim. Acta* **2005**, *358*, 437−443.
(14) Bera, M.; Biradha, K.; Ray, D. *Inorg. Chim. Acta* **2004**, *357*, 3556−3562.
(15) Nanda, P. K.; Mandal, D.; Ray, D. *Polyhedron* **2006**, *25*, 702−710.
(16) Nanda, P. K.; Bera, M.; Aromí, G.; Ray, D. *Polyhedron* **2006**, *25*, 2791−2799.
(17) Fondo, M.; Ocampo, N.; Garcia-Deibe, A. M.; Vicente, R.; Corbella, M.; Bermejo, M. R.; Sanmartín, J. *Inorg. Chem.* **2006**, *45*, 255−262.
(18) Gagne, R. R.; Spiro, C. L.; Smith, T. J.; Hamann, C. A.; Thies, W. R.; Shiemke, A. D. *J. Am. Chem. Soc.* **1981**, *103*, 4073−4081.
(19) Cromie, S.; Launay, F.; McKee, V. *Chem. Commun.* **2001**, 1918−1919.

Scheme 2

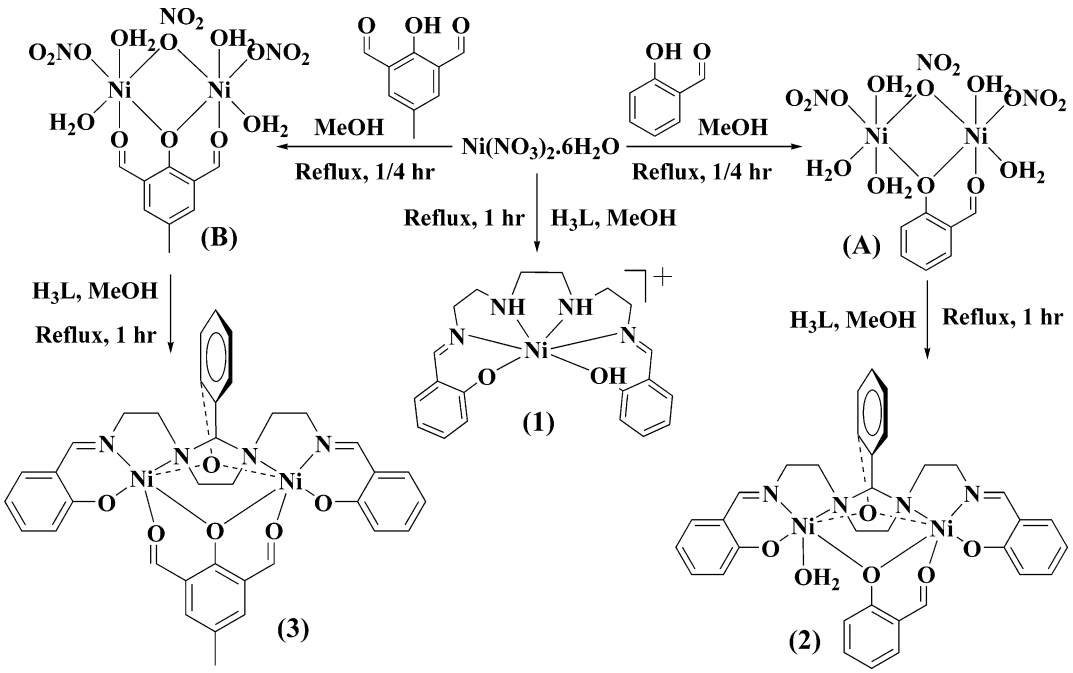

Table 1. Crystallographic Data for Complexes **1**, **2** and **3**

molecular formula	$C_{40}H_{58}N_{10}O_{14}Ni_2$	$C_{34}H_{40}N_4O_9Ni_2$	$C_{36}H_{43}N_4O_{10.5}Ni_2$
molecular weight	1020.33	766.09	817.13
cryst syst	orthorhombic	monoclinic	tetragonal
space group	$Pn2_1a$	$P2_1/c$	$P\bar{4}2_1c$
a (Å)	13.571(2)	11.442(4)	19.923(2)
b (Å)	14.106(6)	21.410(7)	19.923(2)
c (Å)	23.625(3)	14.714(5)	18.511(3)
α (deg)	90.00	90.00	90.00
β (deg)	90.00	101.67(1)	90.00
γ (deg)	90.00	90.00	90.00
U (Å^3)	4522.3(12)	3530.0(21)	7347.2(16)
D_c (g cm^{-3})	1.487	1.441	1.461
Z	8	4	2
F(000)	2112	1600	3344
cryst size (mm)	0.24 × 0.22 × 0.18	0.39 × 0.13 × 0.08	0.44 × 0.28 × 0.14
μ (mm^{-1})	0.909	1.125	1.088
θ range (deg)	1.68−24.97	0.9−27.5	1.45−24.97
R1[a], wR2 [$I > 2\sigma$(I)]	0.0458, 0.1314	0.0460, 0.500	0.0612, 0.1351
GOF on F^2	1.118	1.080	1.023
final difference map max, min (e Å^{-3})	0.509, −0.606	1.10, −0.66	0.519, −0.771

[a] $R1 = \sum(||F_o| - |F_c||)/\sum|F_o|$, $wR2 = [\sum w(|F_o| - |F_c|)^2/\sum w(F_o)^2]^{1/2}$, $w = 0.75/(\sigma^2(F_o) + 0.0010F_o^2)$.

within the complex via the phenolate O donor, and introduces asymmetry by binding to only one Ni atom through its carbonyl moiety. Hexacoordination around the other Ni ion is instead achieved through binding of a molecule of water. Each Ni atom is thus coordinated in a distorted octahedral N_2O_4 environment with the two octahedra sharing the edge defined by the bridging phenolate oxygen atoms (Figure 3). The equatorial planes intersecting at this edge form an angle of 151.41°, as a result of the folding imposed by imidazolidine ring (N2···N3 = 2.296(5) Å). The geometric restrictions resulting from L^{3-} also cause the Ni−O−Ni angles to be different (95.7(1) and 97.8(1)° for endogenous and exogenous phenolate oxygens, respectively). The intramolecular Ni···Ni distance is 3.083 Å. In a very interesting analogy with the active site of urease, the aldehyde carbonyl coordination observed in **2** mimics the coordination of urea to the enzyme (as previously established with several Ni_2 model complexes).[5] The binding of H_2O to the second metal center, parallels the activation of this substrate by urease before the nucleophilic attack to the carbonyl of urea takes place.[5,20−23] The crystal lattice of complex **2** features a network of intermolecular hydrogen bonds between lattice water molecules and both the coordinated water and terminal phenolate oxygens, resulting in a 1D chain of cyclic

(20) Barrios, A. M.; Lippard, S. J. *Inorg. Chem.* **2001**, *40*, 1250−1255.
(21) Barrios, A. M.; Lippard, S. J. *J. Am. Chem. Soc.* **1999**, *121*, 11751−11757.
(22) Konrad, M.; Meyer, F.; Jacobi, A.; Kircher, P.; Rutsch, P.; Zsolnai, L. *Inorg. Chem.* **1999**, *38*, 4559−4566.
(23) Koga, T.; Furutachi, H.; Nakamura, T.; Fukita, N.; Ohba, M.; Takahashi, K.; Okawa, H. *Inorg. Chem.* **1998**, *37*, 989−996.

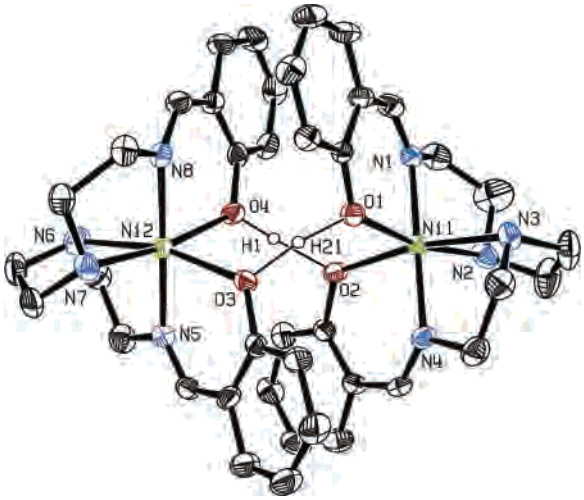

Figure 1. ORTEP representation of the dimer of $[Ni(HL1)]^+$ complexes from **1**, at the 40% probability level. Hydrogen atoms, except these involved in the intradimer H-bonding, are omitted for clarity. Only independent non-carbon atoms are labeled.

Table 2. Selected Interatomic Distances (Å) and Angles (deg) for Complexes **1**, **2**, and **3**

1		**2**		**3**	
Ni1−N4	2.019(6)	Ni1−O1	2.008(4)	Ni1−O1	1.989(9)
Ni1−O1	2.075(5)	Ni1−O2	2.066(3)	Ni1−N1	2.000(9)
Ni1−N3	2.122(7)	Ni1−O4	2.010(3)	Ni1−O4	2.040(7)
Ni1−N1	2.027(6)	Ni1−O5	2.100(3)	Ni1−O2	2.076(9)
Ni1−N2	2.121(6)	Ni1−N1	2.004(4)	Ni1−O5	2.087(9)
Ni1−O2	2.096(5)	Ni1−N2	2.179(4)	Ni1−N2	2.168(11)
Ni2−N8	2.025(7)	Ni2−O2	2.092(3)	Ni2−N4	1.970(12)
Ni2−O3	2.075(5)	Ni2−O3	1.989(4)	Ni2−O3	2.013(9)
Ni2−O4	2.098(5)	Ni2−O4	2.080(3)	Ni2−O4	2.044(8)
Ni2−N6	2.114(7)	Ni2−O6	2.167(3)	Ni2−O2	2.063(7)
Ni2−N5	2.043(7)	Ni2−N3	2.174(4)	Ni2−O6	2.122(9)
Ni2−N7	2.088(6)	Ni2−N4	2.006(4)	Ni2−N3	2.157(11)
N4−Ni1−O2	87.9(2)	O1−Ni1−N1	90.6(2)	O1−Ni1−N1	91.3(4)
N1−Ni1−N2	82.4(3)	O4−Ni1−O5	88.0(1)	O4−Ni1−O2	81.8(3)
N4−Ni1−N3	81.4(3)	O2−Ni1−O4	81.5(1)	O4−Ni1−O5	86.6(3)
N1−Ni1−O1	87.7(2)	N1−Ni1−N2	83.5(2)	N1−Ni1−N2	83.1(5)
O1−Ni1−O2	90.45(19)	O4−Ni2−O6	92.9(1)	N4−Ni2−O3	91.6(5)
N2−Ni1−N3	81.8(3)	Ni1−O2−Ni2	95.7(1)	N4−Ni2−O2	100.6(4)
N8−Ni2−N7	83.8(3)	O2−Ni2−O4	79.2(1)	N4−Ni2−O6	91.4(4)
N8−Ni2−O4	86.1(2)	O2−Ni2−N4	99.1(1)	Ni1−O4−Ni2	96.8(3)
N7−Ni2−N6	81.2(3)	O6−Ni2−N4	88.5(1)	N4−Ni2−N3	83.8(5)
N5−Ni2−O3	86.6(3)	Ni1−O4−Ni2	97.8(1)	Ni2−O2−Ni1	95.1(3)
O3−Ni2−O4	87.73(18)	O3−Ni2−N4	91.7(2)	O4−Ni2−O2	82.0(3)
N5−Ni2−N6	80.0(3)	N3−Ni2−N4	82.9(2)	O4−Ni2−O6	86.0(4)

pentagonal water clusters (one coordinated H_2O per cluster) running along the crystallographic *b*-axis (Figure 4). Cyclic water clusters of five members are an extremely rare form of organization of this molecule within supramolecular networks.[24] In the current case, the pentamers exhibit a "cyclopentane-like" conformation, with one water oxygen (O9W) 0.701 Å below the plane formed by the other O atoms of the cycle (Figure S2).

$[Ni_2(L)(dfp)]\cdot 4.5H_2O$ (3·4.5H_2O). Complex **3** (Figure 5) is a dinuclear aggregate of Ni^{II} ions bridged and chelated by the ligand L^{3-} in the same manner as in complex **2**. The bridging and hexacoordination of both metals is completed by a symmetric 2,6-diformylphenoxide (dfp^-) ligand that binds terminally both metals through each of its carbonyl

(24) Ma, B. Q.; Sun, H. L.; Gao, S. *Chem. Commun.* **2004**, 2220−2221.

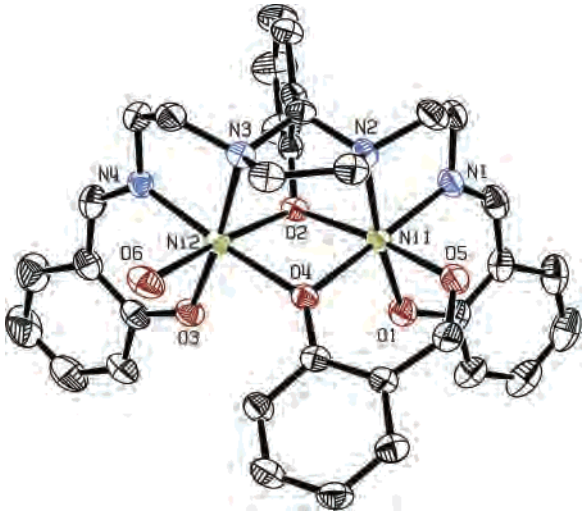

Figure 2. ORTEP representation of $[Ni_2L(fp)(H_2O)]$ (**2**) at the 40% probability level. Hydrogen atoms are omitted for clarity. Only independent non-carbon atoms are labeled.

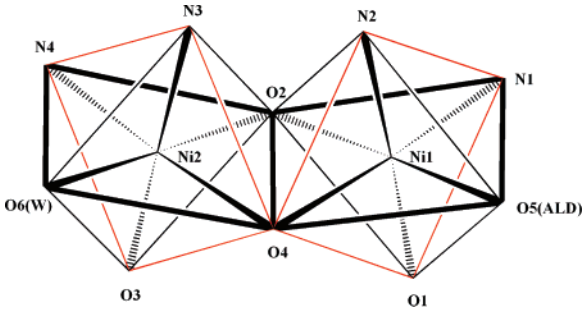

Figure 3. Edge-shared coordination polyhedra around the nickel centers in complex **2**.

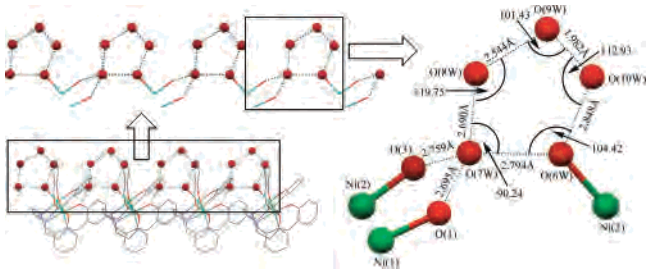

Figure 4. Intermolecular hydrogen-bonded 1D chain of novel pentameric water cluster running along the crystallographic *b*-axis in complex **2**.

groups, respectively, while linking them via the central phenolate μ-O. The tetradentate ligand dfp^- naturally binds the edges offered by the $[Ni_2L]^+$ moiety; therefore, the change of H_2O and fp^- for dfp^- in going from **2** to **3** does not introduce significant changes to the overall metric parameters of the complex. Thus, the dihedral angles between intersecting equatorial planes is here 155.98°; the bridging Ni−O−Ni angles are 95.1(3) (endogenous) and 96.8(3)° (exogenous), and the Ni···Ni separation is 3.054 Å. The angle between the chelate rings of dfp^- is 163.53°. No special hydrogen-bonding network was observed within the crystal lattice of **3**.

Magnetic Properties. The magnetic properties of complexes **1**, **2**, and **3** were investigated by means of bulk magnetization methods. Measurements were collected under

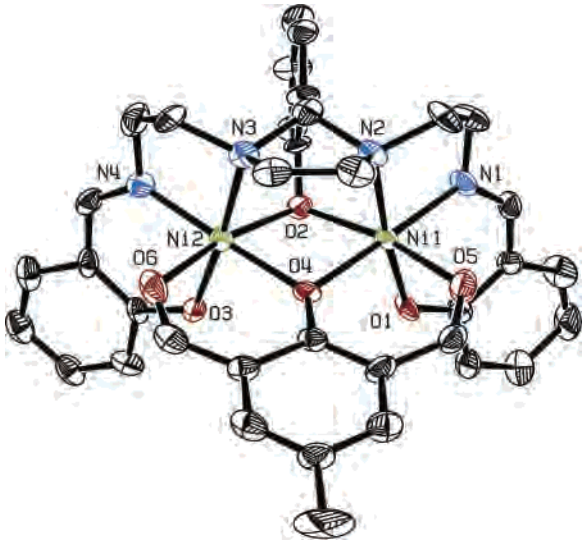

Figure 5. ORTEP representation of [Ni$_2$L(dfp)] (**3**) at the 40% probability level. Hydrogen atoms are omitted for clarity. Only independent non-carbon atoms are labeled.

a constant magnetic field of 7 kG in the 2−300 K temperature range.

The interest in studying the magnetic behavior of **1** is to quantify the possible magnetic exchange between paramagnetic centers as mediated exclusively through hydrogen bonds, something that has been done rarely in molecular magnetism,[25] which has been found, however, to lead to sophisticated effects such as the exchange-biased quantum tunneling of clusters.[26] The results may be represented in form of $\chi_M T$ versus T plots (Figure S3) with χ_M being the molar paramagnetic susceptibility. In this plot, the value of the product $\chi_M T$ at 300 K is 2.27 cm^3 K mol^{-1} (corresponding to two isolated $S = 1$, centers with $g = 2.13$), and it remains constant until near 25 K, where it starts to decrease with cooling, first slightly and then abruptly, down to 1.01 cm^3 K mol^{-1} at 2 K. This behavior is most likely caused by either the weak antiferromagnetic exchange between both Ni^{II} ions through the hydrogen bonds, the zero-field splitting (ZFS) of the metal centers, or both at the same time. Therefore, an appropriate model to simulate these data needs to contemplate these two effects. This was done by full diagonalization of the matrix arising from the spin Hamiltonian $H = -2JS_1S_2 + g\beta(S_1 + S_2) + 2[D_{Ni}(S^2_{Niz} - S_{Ni}(S_{Ni} + 1)/3)]$, where the first term represents the magnetic coupling between the Ni^{II} centers of the dimer ($S_1 = S_2 = 1$), the second term is the Zeeman splitting of the dimer spin states (S_T is the total Ni$_2$ spin), and the third term includes the effect of single ion ZFS (D_{Ni}, which is equal for both Ni ions of **1**) with $S_{Ni} = 1$. An excellent fit (solid line in Figure S1) was obtained for values of $J = -0.3$ cm^{-1}, $D_{Ni} = 4.89$ cm^{-1}, and $g = 2.13$. These results suggest that the exchange coupling through the hydrogen bonds is small but not negligible, as found with the few previous examples studied.[25,26] In the present case, however, these conclusions are to be taken with caution

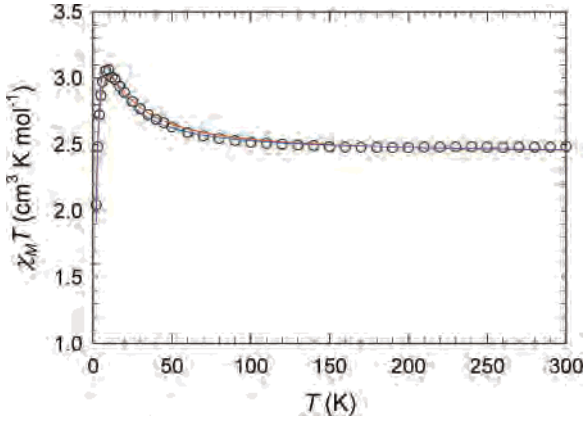

Figure 6. $\chi_M T$ vs T plot for [Ni$_2$L(fp)(H$_2$O)] (**2**). Solid lines are the best fit to the experimental data using two different models (see text for details).

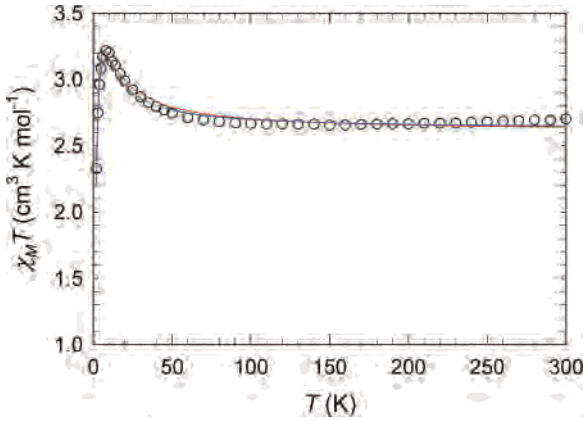

Figure 7. $\chi_M T$ vs T plot for [Ni$_2$L(dfp)] (**3**). Solid lines are the best fit to the experimental data using two different models (see text for details).

because the two parameters modeled here (J and D) are correlated, since their effect on $\chi_M T$ *vs* T is very similar. Nevertheless, the $|D|$ value[27] obtained with this fit is in line with these previously observed by high-field EPR for mononuclear octahedral Ni^{II} centers.[28]

The results for compounds **2** and **3** do not differ very much from each other and are represented in Figures 6 and 7, respectively, also in form of $\chi_M T$ versus T plots. At room temperature, the product $\chi_M T$ is slightly higher than expected for a pair of independent Ni^{II} ions with $g = 2.2$ (this would correspond to 2.42 cm^3 K mol^{-1}), and they increase upon cooling with a more pronounced slope as the temperature becomes closer to zero to reach maxima at 3.1 and 3.2 cm^3 K mol^{-1}, respectively, near 8 K. Below this temperature, an abrupt decrease is observed. The fact that both complexes behave so similarly is expected from the fact that they differ very little in their geometric features and that the bridging of the metals is essentially the same in both cases. The only difference is that instead of terminal H$_2$O, Ni2 in **3** exhibits a second carbonyl, linking this metal to the exogenous phenolate. This does not dramatically affect the Ni···Ni magnetic interaction. The experimental behavior clearly shows that the intermolecular coupling is ferromagnetic,

(25) Valigura, D.; Moncol, J.; Korabik, M.; Púčeková, Z.; Lis, T.; Mroziński, J.; Melník, M. *Eur. J. Inorg. Chem.* **2006**, 3813−3817.
(26) Wernsdorfer, W.; Aliaga-Alcalde, N.; Hendrickson, D. N.; Christou, G. *Nature* **2002**, *416*, 406−409.
(27) Magnetic susceptibility data are quite insensitive to the sign of D; therefore, we give the absolute value here.
(28) Krzystek, J.; Ozarowski, A.; Telser, J. *Coord. Chem. Rev.* **2006**, *250*, 2308−2324.

leading to a ground state of $S = 2$. This is consistent with isothermal reduced magnetization measurements for both complexes (Figures S4 and S5), which indicate saturation at values slightly higher than 4. The decrease of $\chi_M T$ at lower temperatures may be caused by either intermolecular antiferromagnetic interactions or by ZFS of the ground state. These effects have been considered separately by fitting the magnetic data consecutively with two different models, (i) one that includes, in addition to the intramolecular coupling, interactions between the $S = 2$ spin centers, and (ii) a second one that contemplates the Ni···Ni superexchange and the single ion ZFS term of the Ni^{II} centers (which ultimately causes the overall ZFS of the dimer) as done above for complex **1**.

The first model involves the use of a $\chi_M = f(T)$ expression[29] derived from the isotropic Hamiltonian $H = -2JS_1S_2 + g\beta S_{Tz} + zJ' < S_{Tz} > S_{Tz}$. In this Hamiltonian,[30] the first two terms are the same as with the above model and the third term accounts for the weak intermolecular interactions (J' is the constant of the coupling between first neighbors and z is the number of such neighbors per molecule). The fit (red lines in Figures 6 and 7) provided the following parameters (in the **2**/**3** format): $J = +3.4/+2.4$ cm^{-1}, $g = 2.20/2.28$, and $zJ' = -0.5/-0.4$ cm^{-1}. The small and ferromagnetic intramolecular coupling might be ascribed to the Ni−O−Ni angles formed by the phenolate bridges (between 95 and 98°),[31] which are within the range predicted to lead to ferromagnetic interactions in this metal, or to the imidazolidine −NCN− bridge, which also has been shown to facilitate ferromagnetic Ni···Ni exchange.[29] The second model was applied by full diagonalization of the matrix arising from the same spin Hamiltonian as used for complex **1**. This method provided similar but slightly better fits than the previous one (red lines in Figures 6 and 7). The parameters emerging from this fit are $J = +2.3/+1.5$ cm^{-1}, $g = 2.20/2.29$, and $|D_{Ni}| = 6.4/5.2$ cm^{-1}. The values of J obtained here are slightly smaller than for the previous model, and the single-ion $|D_{Ni}|$ values are on the same order as in complex **1**. The isothermal reduced magnetization data for complexes **2** and **3** were also fit using this model, by means of a full diagonalization method, to compare the D_{Ni} values obtained from two different kinds of fitting. The parameters obtained are 5.2 and 4.5 cm^{-1} for **2** and **3**, respectively, while the parameters J and g were fixed at the values obtained with the above fit.

Conclusions

As part of the interesting chemistry of the ligand L^{3-} with Ni^{II}, we have shown that external addition of formylphenol or diformylphenol to the system inhibits the hydrolysis of the former and leads to the high yield formation of the assemblies $[Ni_2(L)(fp)(H_2O)]$ (**2**) and $[Ni_2(L)(dfp)]$ (**3**). The crystal structure of **2** shows that this complex is a structural model of the active site of urease, featuring a carbonyl moiety (mimicking urea) coordinated to one Ni^{II} and one molecule of water to the other Ni^{II} center. Magnetic measurements indicate that the dimer of monomers **1** may exhibit weak antiferromagnetic coupling between the Ni^{II} centers through hydrogen bonds, whereas complexes **2** and **3** feature ferromagnetic super-exchange, and $S = 2$ ground states. The bulk magnetic properties were modeled by consideration of the exchange coupling and either antiferromagnetic interactions or single ion zero field splitting. We are currently working to exploit the asymmetry induced by external bridges in this reaction system to induce the formation of heterometallic complexes. Athough complex **2** is a good structural mimic of urease (with one water and one carbonyl group bound to the Ni centers), it exhibits ferromagnetism as compared to weakly antiferromagnetically coupled Ni centers in urease, which clearly indicates, the architecture of the Ni sites requires fine-tuning.

Experimental Section

Syntheses. The chemicals used were obtained from the following sources: triethylenetetramine from S.D. Fine Chem (India), 2-formyl phenol from SRL (India), 2,6-diformyl 4-methyl phenol prepared following the literature procedure,[18] and nickel nitrate hexahydrate from Spectrochem (India). All other chemicals and solvents were reagent grade materials and were used as received without further purification.

$[Ni(HL1)]_2(NO_3)_2$ (1). Ligand H_3L (0.5 g, 1.09 mmol) in hot methanol (30 mL) was added to a methanolic solution (50 mL) of $Ni(NO_3)_2 \cdot 6H_2O$ (0.633 g, 2.18 mmol), and the mixture was refluxed for 1 h. The resulting solution was allowed to cool to room temperature, filtered, and left to slowly evaporate. After 4 days, a reddish brown crystalline product was obtained (~60% yield). The solid was isolated, washed with cold methanol, and dried under vacuum over P_4O_{10}. Anal. Calcd for $\mathbf{1} \cdot 4H_2O$ ($C_{40}H_{58}N_{10}Ni_2O_{14}$, MW = 1020.33): C, 47.08; H, 5.73; N, 13.72. Found: C, 46.88; H, 5.46; N, 13.12. Molar conductance, Λ_M (MeCN solution): 232 ohm^{-1} cm^2 mol^{-1}. UV−vis spectrum (MeCN): λ_{max} (ϵ_{max}) 842 (210), 321 (10104). Selected IR bands (KBr, cm^{-1}): 3401 vs, 3056 m, 2918 w, 1641 s, 1600 s, 1451 m, 1384 s, 1286 w, 1123 m, 758 s.

$[Ni_2L(fp)(H_2O)]$ (2). 2-Formyl phenol (0.116 mL, 1.09 mmol) was added dropwise for 15 min to a refluxed methanolic solution (50 mL) of $Ni(NO_3)_2 \cdot 6H_2O$ (0.633 g, 2.18 mmol). Ligand H_3L (0.5 g, 1.09 mmol) in hot methanol (20 mL) was added to the resulting solution, and the mixture was refluxed for 1 h. The resulting solution was allowed to cool to room temperature, filtered, and left undisturbed to slowly evaporate. After 3 days, a green crystalline product was obtained (~76% yield). The solid was isolated, washed with cold methanol, and dried under vacuum over P_4O_{10}. Anal. Calcd for $\mathbf{2} \cdot 3H_2O$ ($C_{34}H_{40}N_4Ni_2O_9$; MW = 766.091): C, 53.30; H, 5.26; N, 7.31. Found: C, 52.98; H, 5.48; N, 6.92. Molar conductance, Λ_M (MeCN solution): 10 ohm^{-1} cm^2 mol^{-1}. UV−vis spectrum (MeCN): λ_{max} (ϵ_{max}) 924 (216), 780 (25), 597 (140), 369 (13120), 249 (28450). Selected IR bands (KBr, cm^{-1}): 3267 s, 2918 w, 1642 s, 1600 s, 1535 m, 1483 s, 1467 s, 1445 s, 1320 m, 1289 m, 1151 s, 1128 s, 1105 s, 1032 s, 937 m, 756 s, 639 m, 586 w.

$[Ni_2L(dfp)]$ (3). 2,6-Diformyl 4-methyl phenol (0.178 g, 1.09 mmol) in methanol (20 mL) was added dropwise to a methanolic solution (50 mL) of $Ni(NO_3)_2 \cdot 6H_2O$ (0.633 g, 2.18 mmol), and the

(29) Fondo, M.; García-Deibe, A. M.; Ocampo, N.; Sanmartín, J.; Bermejo, M. R.; Llamas-Saiz, A. L. *Dalton Trans.* **2006**, 4260−4270.
(30) Kahn, O. In *Molecular Magnetism*; VCH: New York, 1993; p 131.
(31) Nanda, K. K.; Thompson, L. K.; Bridson, J. N.; Nag, K. *J. Chem. Soc., Chem. Commun.* **1994**, 1337−1338.

mixture was refluxed for 15 min. Ligand H_3L (0.5 g, 1.09 mmol) in hot methanol was added to the resulting solution, and the mixture was refluxed for 1 h. Then the resulting solution was allowed to cool to room temperature, filtered, and left for slow evaporation. After 6 days, a green crystalline product was obtained (~79% yield). The solid was isolated, washed with cold methanol, and dried under vacuum over P_4O_{10}. Anal. Calcd for **3**·4.5H_2O ($C_{36}H_{43}N_4Ni_2O_{10.5}$; MW = 817.1362): C, 52.91; H, 5.30; N, 6.85. Found: C, 52.88; H, 5.48; N, 6.66. Molar conductance, Λ_M (MeCN solution): 10 ohm^{-1} cm^2 mol^{-1}. UV−vis spectrum (MeCN): λ_{max} (ϵ_{max}) 900 (310), 783 (30), 590 (210), 386 (14020), 259 (29600). Selected IR bands (KBr, cm^{-1}): 3268 s, 1657 s, 1639 s, 1598 s, 1530 s, 1468 s, 1449 s, 1403 m, 1346 s, 1322 w, 1231 w, 1189 w, 1149 w, 1107 w, 1037 m, 992 m, 756 m, 561 m.

X-ray Crystallography. The deep green blocklike single crystals of **1** suitable for the X-ray analysis were grown by the slow evaporation of a MeCN solution of the complex. Similarly, platelike single crystals of **2** and **3** suitable for X-ray analysis were grown by the slow evaporation of a MeCN/CH_2Cl_2 (1:1) solutions of the complexes during a week. Information concerning the X-ray data collection and structure refinement of the compound is summarized in Table 1. The intensity data of the complex **1** and **3** were collected on Nonius CAD4 X-ray diffractometer that uses graphite-monochromated Mo Kα radiation (λ = 0.71073 Å) by ω-scan method. Similarly, data for complex **2** was collected on Bruker SMART CCD single-crystal X-ray diffractometer. Data were collected at 293 K for complexes **1** and **3** and for complex **2** at 303 K. For complex **1**, total of 4147 reflections were recorded with Miller indices $h_{min} = 0$, $h_{max} = 16$, $k_{min} = 0$, $k_{max} = 16$, $l_{min} = 0$, $l_{max} = 28$. For complex **2**, a total of 22317 reflections were recorded with Miller indices $h_{min} = -14$, $h_{max} = 14$, $k_{min} = -22$, $k_{max} = 27$, $l_{min} = -19$, $l_{max} = 18$. For complex **3**, a total of 3534 reflections were recorded with Miller indices $h_{min} = 0$, $h_{max} = 23$, $k_{min} = 0$, $k_{max} = 23$, $l_{min} = 0$, $l_{max} = 21$. In the final cycles of full-matrix least-squares on F^2, all non-hydrogen atoms were assigned anisotropic thermal parameters. The positions of the H atoms bonded to C atoms were calculated (C−H distance 0.97 Å). The structure was solved using the program SHELX-97[32] and refined by full-matrix least-squares methods with use of the program SHELX-97. The CCDC numbers corresponding to complexes **1**, **2**, and **3** are 637395, 279652, and 290927, respectively.

Physical Measurements. The elemental analyses (C, H, N) were performed with a Perkin-Elmer model 240 C elemental analyzer. IR spectra were recorded on a Perkin-Elmer 883 spectrophotometer. The solution electrical conductivity and electronic spectra were obtained using a Unitech type U131C digital conductivity meter with a solute concentration of about 10^{-3} M and a Shimadzu UV 3100 UV−vis−NIR spectrophotometer respectively. The room-temperature magnetic susceptibilities in the solid state were measured using a home-built Gouy balance fitted with a polytronic dc power supply. Magnetic measurements were carried out in the "Servei de Magnetoquímica (Universitat de Barcelona)" on polycrystalline samples (~30 mg) using a Quantum Design MPMS XL-5 SQUID susceptometer, operating at a constant magnetic field of 0.7 T between 2 and 300 K. The experimental magnetic moment was corrected for the diamagnetic contribution from the sample holder and the diamagnetic response from the sample, which was evaluated from Pascal's constants.

Acknowledgment. We are thankful to the Council of Scientific and Industrial Research, New Delhi, India, for the financial support. W.T.W. acknowledges the financial support from the Hong Kong government, and G.A. thanks the Spanish Ministry of Science for a "Ramón y Cajal" contract.

Note Added after ASAP Publication. This article was released ASAP on June 15, 2007, with missing CIF files. The correct version was posted on June 19, 2007.

Supporting Information Available: X-ray crystallographic data in CIF format and additional figures showing hydrogen bonding, the water cluster plane, and $\chi_M T$ versus T plots. This material is available free of charge via the Internet at http://pubs.acs.org.

IC700496C

(32) Sheldrick, G. M. *SHELX-97*; Bruker AXS, Madison, WI, 1997.